Attenuation Due to Ohmic Losses in Periodic Dipole and Slot Arrays

NOACH AMITAY, MEMBER, IEEE, AND HENRY ZUCKER, MEMBER, IEEE

Abstract—**The analysis of the attenuation due to ohmic losses in periodic linear arrays of metallic cylinders, ribbons, and slots in a metallic ground plane is presented.**

Calculations indicate that the loss per unit length of the ribbon and cylinder arrays is comparable to that of a standard rectangular waveguide operated in the TE_{10} mode. With a proper choice of parameters, the loss per unit length of the slot array can be brought to within a factor of 2 of that of rectangular waveguides.

I. Introduction

RECENT THEORETICAL and experimental investigations [1]–[8] have shown that a periodic linear array of cylindrical- or ribbon-shaped metallic elements (Fig. 1) may be used as guided-wave transmission lines, filters, and resonators.

Fig. 2(a) shows an array of slots in a thin and conducting infinite ground plane. This slot array is the electromagnetic dual [9] of the ribbon array of Fig. 1(b). The electromagnetic fields of such surface waves decay exponentially away from the slots in the x and y directions. Therefore, for a sufficiently large distance l (typically few wavelengths) from the edge of the slot, the infinite metallic ground plane can be replaced by a strip of width $(2l+2h)$ (see Fig. 2(b)) without affecting the surface-wave propagation.

The potential use of these periodic structures as transmission lines, filters, resonators, etc., depends to a large extent upon their attenuation characteristics due to ohmic losses.

In this work we shall evaluate the relative power loss per unit length in the conducting cylindrical and ribbon arrays shown in Fig. 1, and the slot array of Fig. 2(a). The dispersion characteristics and the currents in these structures that are utilized here are based on previous analyses with the simplifying assumptions therein. The electromagnetic fields are obtained under the assumption of perfectly conducting metal, with the ohmic losses calculated as a first-order perturbation. [10]

A harmonic time variation of exp $[-j\omega t]$ is assumed throughout this work.

II. The Conducting Ribbon Array

A. General Formulation

For a wave propagating in the $+z$ direction and bound to the structure of Fig. 1(b), a current sheet $I(x, z)$ will be induced on the metallic strips. This current sheet will have x and z components on the strips, and vanish outside the strips. Utilizing Floquet's theorem [9] for this periodic structure, we can express $I(x, z)$ as

$$I(x, z) = \sum_{m=-\infty}^{\infty} I_m(x) \exp\ (j\beta_m z), \qquad \beta_m = \beta - \frac{2m\pi}{d} \tag{1}$$

with β being the z-directed propagation constant and with $I(x, z) = 0$ over $|x| > h$ or $|z| > a$ in the periodic cell defined by $-\infty < x < \infty$; $-d/2 < z < d/2$. The vector Fourier coefficients I_m are given by

$$\begin{aligned} I_m(x) &= \hat{x} I_{mx}(x) + \hat{z} I_{mz}(x) \\ &= \frac{1}{d} \int_{-a}^{a} I(x, z) \exp\ (-j\beta_m z) dz \end{aligned} \tag{2}$$

where $\hat{x}$ and $\hat{z}$ are unit vectors in the x and z directions, respectively. We relate the magnetic field $\boldsymbol{H}$, and the electric field $\boldsymbol{E}$ to the vector potential $\boldsymbol{A}$ by

$$\left.\begin{aligned} H &= \frac{1}{\mu} \nabla \times A \\ E &= j\omega \left[A + \frac{1}{k^2} \nabla\nabla \cdot A \right] \end{aligned}\right\} \tag{3}$$

employing the Lorentz gauge. Utilizing the free-space

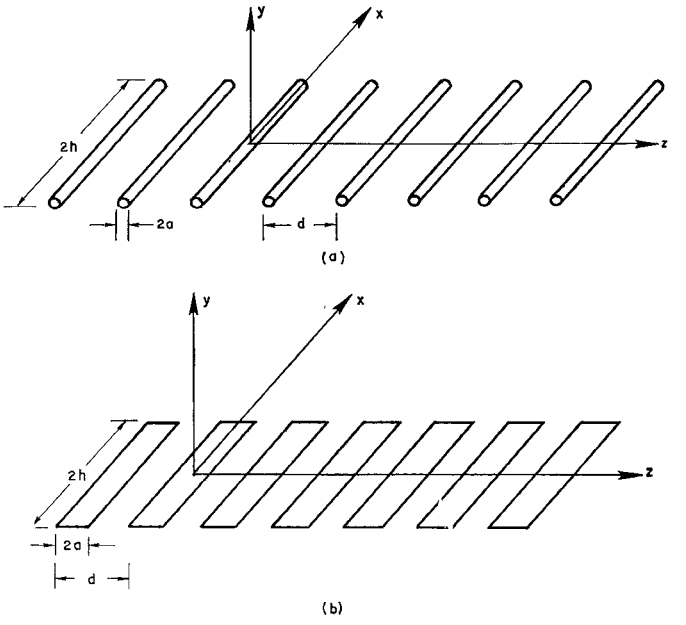

Fig. 1. (a) Array of conducting cylinders. (b) Array of conducting ribbons.

Manuscript received February 19, 1971; revised April 26, 1971.
The authors are with Bell Telephone Laboratories, Inc., Whippany, N. J. 07981.

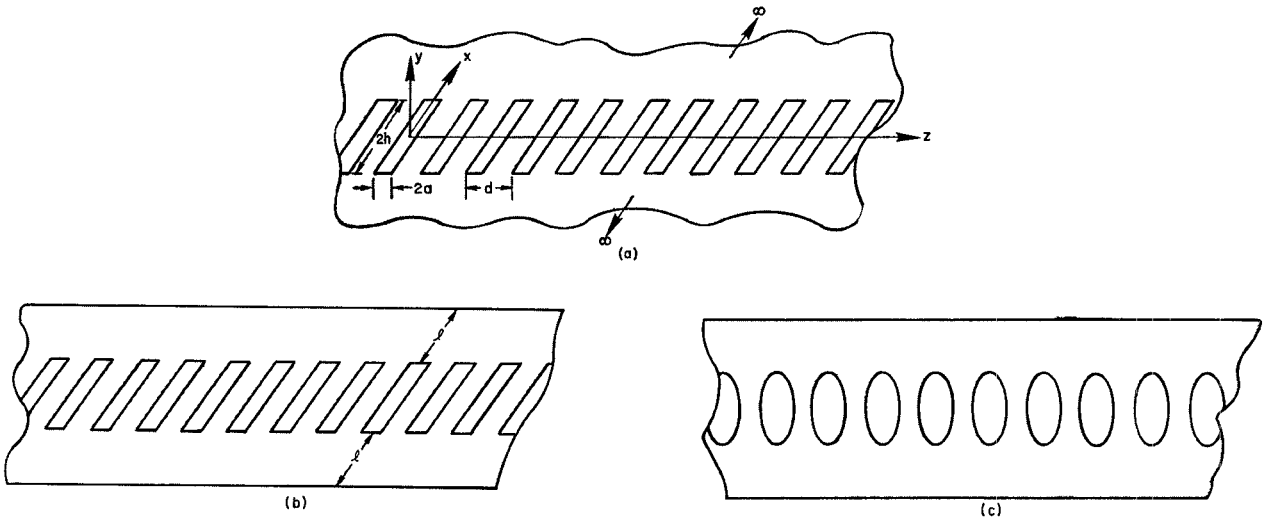

Fig. 2. (a) Slots in a thin and infinite ground plane. (b) Finite slot array. (c) Alternative finite slot array.

Green's function [9] and the Poisson summation formula [11] we can relate [4] the vector potential to the current sheet by

$$A = \frac{\mu}{2\pi d}\sum_{m=-\infty}^{\infty}\int_{x=-h}^{h}\int_{z=-d/2}^{d/2}\exp\left(j\beta_m(z-z')\right) \cdot K_0[\alpha_m\sqrt{(x-x')^2+y^2}]I(x',z')dx'dz' \quad (4)$$

with $\alpha_m=[(\beta-2m\pi/d)^2-k^2]^{1/2}$, $k=2\pi/\lambda$ being the free-space propagation constant, and K_0 denoting the modified Bessel function of the second kind. For a bounded loss-free wave, all $\{\alpha_m\}$ are real, i.e.,

$$|\beta-2m\pi/d| > k, \qquad \text{for all } m. \quad (5)$$

Substituting (2) in (4), we obtain

$$A = \frac{\mu}{2\pi}\sum_{m=-\infty}^{\infty}\exp(j\beta_m z)\int_{-h}^{h}K_0[\alpha_m\sqrt{(x-x')^2+y^2}] \cdot\{\hat{x}I_{mx}(x')+\hat{z}I_{mz}(x')\}dx'. \quad (6)$$

The behavior of $\boldsymbol{A}$ (and thereby the electromagnetic field) far away from the ribbons is given by the asymptotic expansion of K_0 for large arguments. The decay of the mth term in (6) is essentially exponential.

Using the convolution (Faltung) theorem, [11] we can rewrite (6) as

$$A = \frac{\mu}{\sqrt{8\pi}}\sum_{m=-\infty}^{\infty}\exp(j\beta_m z)\int_{t=-\infty}^{\infty}\frac{\exp(-\sqrt{\alpha_m^2+t^2}\,|y|)}{\sqrt{\alpha_m^2+t^2}} \cdot\{\hat{x}l_{mx}(t)+\hat{z}l_{mz}(t)\}\exp(-jtx)dt \quad (7)$$

with the following definition of the Fourier transform

$$l_{mx}(t) = \frac{1}{\sqrt{2\pi}}\int_{-\infty}^{\infty}I_{mx}(x)\exp(jtx)dx = \mathfrak{F}\{I_{mx}(x)\}. \quad (8)$$

We shall assume that both β and $I(x, z)$ have been properly calculated such that $\boldsymbol{E}_t=\hat{x}E_x+\hat{z}E_z$ vanish on the metallic strips.

B. Power-Loss Relationships

To obtain the ohmic loss per unit length we shall assume that the thickness of the ribbon is a few times the skin depth and that the power carried by the bounded wave P_z is constant over a unit cell. The latter is a reasonable approximation when the losses per unit cell P_d are reasonably low [10]. We define

$$P_r = 10p_r\log_{10}e\{\text{dB/unit length}\}, \qquad p_r = \frac{1}{d}\frac{P_d}{P_z}. \quad (9)$$

Under the previous assumptions and the fact that $\boldsymbol{H}_t|_{y=0}=0$ outside the metallic ribbon, we can express P_d as [9], [10]

$$P_d = 2\left\{\frac{1}{2}\int_{x=-h}^{h}\int_{z=-d/2}^{d/2}|\boldsymbol{H}_t|_{y=0}^2R_s dxdz\right\}$$

$$R_s = \sqrt{\frac{\omega\mu}{2\sigma}} \quad (10)$$

with σ being the conductivity of the metal. The power carried by the bounded wave is

$$P_z = \frac{1}{2}\operatorname{Re}\left\{\int_{x=-\infty}^{\infty}\int_{y=-\infty}^{\infty}\boldsymbol{E}\times\boldsymbol{H}^*\cdot\hat{z}dxdy\right\}. \quad (11)$$

For a bounded wave (i.e., *all* α_m are real), it is shown in the Appendix that the electromagnetic fields inherently conserve energy and P_z is constant.

C. Power Loss in Narrow Ribbons or Thin Cylinders

If $a/h\ll 1$, corresponding to narrow ribbons or thin cylinders, the current and the vector potential have essentially an x-directed component only [3]–[6]. We

shall further assume [6] that the current I_x can be expressed by the following product form

$$I_x = F(x)G(z) = F(x) \sum_{m=-\infty}^{\infty} g_m \exp(j\beta_m z),$$

$$\beta_m = \beta - \frac{2m\pi}{d}. \quad (12)$$

Setting $l_{mz}=0$ in (39), we obtain

$$P_z = \frac{\omega\mu}{8k^2} \sum_{m=-\infty}^{\infty} \beta_m |g_m|^2 \int_{-\infty}^{\infty} \frac{(k^2 - t^2)|f(t)|^2}{[\beta_m{}^2 - k^2 + t^2]^{3/2}} dt \quad (13)$$

where $f(t)$ is the Fourier transform of $F(x)$. Utilizing (9), (10), (12), and (13), we obtain the relative power loss p_r as

$$p_r = \frac{8R_s \left(\frac{1}{4}\int_{-h}^{h} |F(x)|^2 dx\right) \sum_{m=-\infty}^{\infty} |g_m|^2}{D^2\sqrt{\mu/\epsilon} \sum_{m=-\infty}^{\infty} (\beta d - 2m\pi)|g_m|^2 \int_{-\infty}^{\infty} \frac{(1-y^2)|f(ky)|^2}{[(\beta d - 2m\pi)^2 + D^2(y^2-1)]^{3/2}} dy} \quad (14)$$

with $D=kd$ and $t=ky$.

III. The Slot Array

A. Analogous Formulation

As was previously stated, the slot array of Fig. 2(a) is the dual structure of the ribbon array of Fig. 1(b). We replace the vector potential $\boldsymbol{A}$ by $\boldsymbol{A}_s$, which is related to the electric field by

$$\boldsymbol{E} = \frac{1}{\epsilon} \nabla \times \boldsymbol{A}_s. \quad (15)$$

The vector potential is related to a fictitious magnetic current sheet $\boldsymbol{I}^s$ in the slot by

$$A_s = \frac{\epsilon}{2\pi} \sum_{n=-\infty}^{\infty} \cdot \exp(j\beta_n z) \int_{-h}^{h} K_0[\alpha_n\sqrt{(x-x')^2 + y^2}] I_n{}^s(x')dx'. \quad (16)$$

The electromagnetic field can be derived from (15) and (16) with a proper gauge [9] or, alternatively, [9] by replacing in (3) $\boldsymbol{A}$ by $\boldsymbol{A}_s$, $\boldsymbol{E}$ by $\boldsymbol{H}$, $\boldsymbol{H}$ by $(-\boldsymbol{E})$, and μ by ϵ. The boundary conditions must also be interchanged.

B. Power Loss in the Narrow-Slot Array

Again, we shall assume narrow slots $a/h \ll 1$, and that the ground plane is a few skin depths thick. With $\boldsymbol{I}^s$ being similar in form to I_x in (12), we obtain P_z by duality from (13) as

$$P_z = \frac{D^2}{8}\sqrt{\frac{\epsilon}{\mu}} \sum_{n=-\infty}^{\infty} (\beta d - 2n\pi)|g_n|^2 \cdot \int_{-\infty}^{\infty} \frac{(1-y^2)|f(ky)|^2}{[(\beta d - 2n\pi)^2 + D^2(y^2-1)]^{3/2}} dy. \quad (17)$$

The power loss per unit cell is

$$P_d = R_s \int_{-\infty}^{\infty} \int_{-d/2}^{d/2} \{|H_x|^2 + |H_z|^2\}\Big|_{y=0} dxdz.$$

Using the appropriate dual expressions of (33) in the equation for P_d and the identity $\beta_m{}^2 = \alpha_m{}^2 + t^2 + (k^2 - t^2)$, one readily obtains

$$P_d = \frac{\epsilon d R_s}{4\mu}\left\{\sum_{m=-\infty}^{\infty} \frac{|g_m|^2}{k^2} \int_{-\infty}^{\infty} |tf(t)|^2 dt + \sum_{m=-\infty}^{\infty} |g_m|^2 \int_{-\infty}^{\infty} \frac{(k^2 - t^2)|f(t)|^2}{\alpha_m{}^2 + t^2} dt\right\}. \quad (18)$$

Substituting (17) and (18) in (9) and utilizing Parseval's theorem, we obtain the relative power loss p_s as

$$p_s = \frac{1}{d}\frac{P_d}{P_z} = \frac{2R_s}{D^2\sqrt{\frac{\mu}{\epsilon}}} \cdot \frac{\frac{1}{k^2}\sum_{m=-\infty}^{\infty} |g_m|^2 \int_{-h}^{h} \left|\frac{dF(x)}{dx}\right|^2 dx + D^2 k \sum_{m=-\infty}^{\infty} |g_m|^2 \int_{-\infty}^{\infty} \frac{(1-y^2)|f(ky)|^2}{[(\beta d - 2m\pi)^2 + D^2(y^2-1)]} dy}{\sum_{m=-\infty}^{\infty} (\beta d - 2m\pi)|g_m|^2 \int_{-\infty}^{\infty} \frac{(1-y^2)|f(ky)|^2}{[(\beta d - 2m\pi)^2 + D^2(y^2-1)]^{3/2}} dy} \quad (19)$$

with $P_s = 10p_s \log_{10} e\{\text{dB/unit length}\}$. The ratio of the power losses per unit length of the ribbon and slot arrays is therefore

$$\eta = \frac{p_s}{p_r} = \frac{P_3}{P_r} = \frac{\frac{1}{k^2}\int_{-h}^{h} \left|\frac{dF(x)}{dx}\right|^2 dx \left[\sum_{m=-\infty}^{\infty} |g_m|^2\right] + D^2 k \sum_{m=-\infty}^{\infty} |g_m|^2 \int_{-\infty}^{\infty} \frac{(1-y^2)|f(ky)|^2}{[(\beta d - 2m\pi)^2 + D^2(y^2-1)]} dy}{\int_{-h}^{h} |F(x)|^2 dx \left[\sum_{m=-\infty}^{\infty} |g_m|^2\right]}. \quad (20)$$

In (14), (19), and (20), if sharp edges are assumed, the expressions for the currents in the metal have singularities that are nonsquare integrable with

$$\lim_{m\to\infty} |g_m|^2 \sim \frac{1}{m}.$$

Thus the first term in the numerator of (20) diverges while the second term is finite. Even if the edges are rounded, the second term is likely to be much smaller than the first. Therefore, we shall approximate (20) by

$$\eta = \frac{p_s}{p_r} \simeq \frac{1/k^2 \int_{-h}^{h} \left|\frac{dF(x)}{dx}\right|^2 dx}{\int_{-h}^{h} |F(x)|^2 dx}. \tag{21}$$

IV. Evaluation of the Power Losses in Ribbon and Slot Arrays

As seen from (14), p_r is dependent on the current distribution and propagation constant β which has been studied previously [3]–[7]. Despite the different formulations and assumptions, these results show similar characteristics and can be used to obtain useful information for our purposes. Present data are restricted to the lowest order mode of the structures.

The current sheet in the ribbon array is of the form of (12), and is taken as [3], [6], [7]

$$I = (\cos kx - \cos kh)\sqrt{\frac{2}{\cos\frac{2\pi z}{d} - \cos\frac{2\pi a}{d}}} \cdot \exp\left(j(\beta d - \pi)(z/d)\right), \quad \text{for } |x| < h \text{ and } |z| < a. \tag{22}$$

This current satisfies the edge conditions, i.e., $I(x = \mp h) = 0$ and

$$\lim_{|z|\to a} I \sim (a - |z|)^{-1/2}.$$

For this current, we find [6], [12]

$$F(x) = \cos kx - \cos kh$$

$$g_m = \begin{cases} P_{m-1}\left(\cos\frac{2\pi a}{d}\right), & m > 0 \\ P_{-m}\left(\cos\frac{2\pi a}{d}\right), & m \le 0 \end{cases} \tag{23}$$

where the P_m are Legendre polynomials.

In order to avoid the singularities of the current at $z = \mp a$, we shall assume that these edges are rounded in the shape of a semicircle of radius δa, as shown in Fig. 3. While the z variation of the current follows (22) in the interval $-a(1-\delta) < z < a(1-\delta)$, the current along the semicircles is assumed to be constant and equal to the current at $z = (1-\delta)a$. In this representation, $\delta = 1$ corresponds to the cylindrical conductor array with uniform current distribution. We calculate the power loss per unit cell from (10) and (22) as

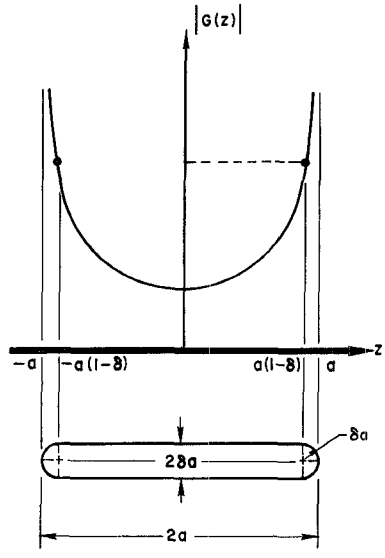

Fig. 3. Ribbon array. Current sheet distribution in the z direction.

$$P_d = \frac{R_s h d}{2\pi} M_2 M_3 \tag{24}$$

with $M_2 = 2 + \cos 2H - 3 \sin 2H/2H$, $H = kh$, $u_0 = 2\pi a/d$, and

$$M_3 = \frac{\pi}{2} \frac{u_0\delta}{\cos[u_0(1-\delta)] - \cos u_0} + \frac{1}{\sin u_0} \cdot \ln \left| \frac{(1+\cos u_0)\tan\left[\frac{u_0}{2}(1-\delta)\right] + \sin u_0}{(1+\cos u_0)\tan\left[\frac{u_0}{2}(1-\delta)\right] - \sin u_0} \right|.$$

We obtain P_z from (13) and (23) as

$$P_z = \frac{2D^2H^2}{4k^2\pi} M_1 \sqrt{\frac{\mu}{\epsilon}} \tag{25}$$

with

$$M_1 = \sum_{m=-\infty}^{\infty} |g_m|^2(\beta d - 2m\pi) \cdot \int_0^{\infty} \frac{\left[\cos H \frac{\sin Hy}{Hy} - \cos Hy \frac{\sin H}{H}\right]^2}{(1-y^2)[(\beta d - 2m\pi)^2 + D^2(y^2-1)]^{3/2}} dy.$$

The relative power loss per unit length is therefore

$$p_r = \frac{1}{\lambda} \frac{R_s}{\sqrt{\frac{\mu}{\epsilon}}} \frac{2\pi M_2 M_3}{H D^2 M_1}. \tag{26}$$

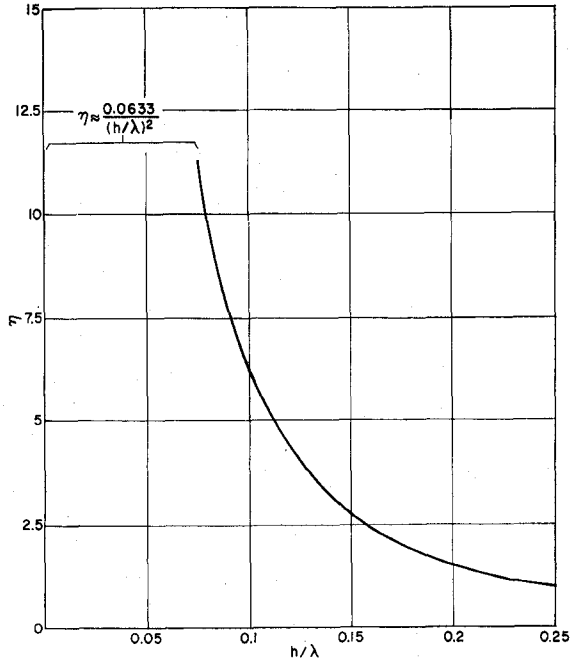

Fig. 4. Ratio of relative loss between the slot and ribbon array versus h/λ.

For the slot array of Fig. 2(a), we utilize (21), (23), and (26) and obtain

$$p_s = \eta p_r, \quad \text{with } \eta = \frac{1 - \sin 2H/2H}{2 + \cos 2H - 3 \sin 2H/2H}. \tag{27}$$

Fig. 4 shows η versus h/λ. In the propagation band of the lowest order mode (i.e., $h/\lambda < 0.25$), the narrow-slot array is lossier than the ribbon array.

A further and more instructive comparison can be made with the TE_{10} mode in standard-rigid-rectangular waveguides for which the power loss per unit length is [10]

$$P_w = 10 p_w \log_{10} e \{\text{dB/unit length}\}$$

$$\frac{6.32}{\lambda} R_s/\sqrt{\mu/\epsilon} \leq p_w \leq \frac{15.33}{\lambda} R_s/\sqrt{\mu/\epsilon}. \tag{28}$$

Note from (26) and (28) that the losses in the ribbon and slot arrays and the dominant waveguide mode have the *same frequency scaling characteristics.*

To compare the relative losses of the various arrays, we define the excess loss factors above the minimum loss per unit length of rectangular waveguides as

$$L_r = \frac{p_r}{6.32 \dfrac{R_s}{\lambda \sqrt{\dfrac{\mu}{\epsilon}}}}$$

$$L_s = \eta L_r. \tag{29}$$

An important parameter in the analysis of the bounded (slow) wave structure is the ratio of the phase velocity of the bounded wave to the velocity of light, v/c. The propagation constant of the bounded wave β is related to v/c by $\beta d = kd/(v/c)$. We shall utilize published values [3]–[6] of v/c in various structures and calculate the corresponding excess loss factors from (29).

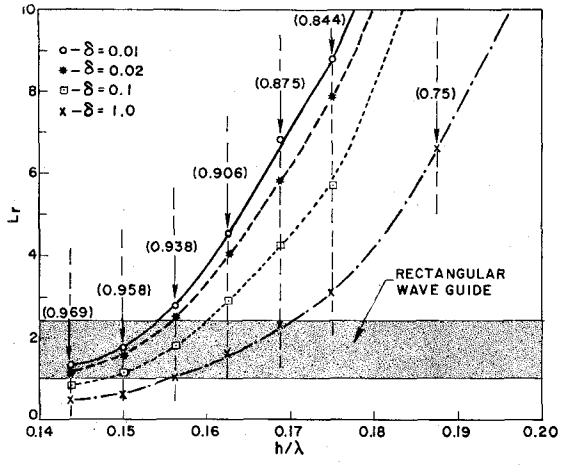

Fig. 5. Excess loss factor L_r for the ribbon array. $h/d = 4$; $2a/d = 0.415$. Corresponding values of v/c are in brackets.

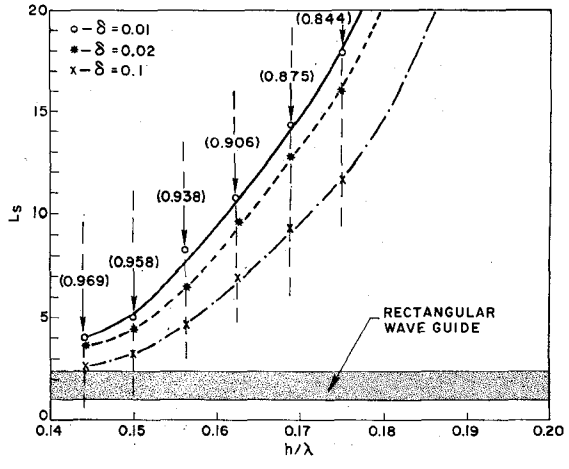

Fig. 6. Excess loss factor for the slot array. $h/d = 4$; $2a/d = 0.415$. Corresponding values of v/c are in brackets.

Fig. 5 shows the factor L_r plotted as a function of h/λ for various ribbon geometries (see Figs. 1(b) and 3). The dispersion characteristics were taken from Ivanov [6] and are assumed independent of δ. As can be seen, L_r increases with decreasing v/c. L_r also increases with the sharpness of the edges (lower values of δ). For a given value of v/c, the lowest losses are incurred by the metallic cylinder array ($\delta = 1$). As can be seen, the losses of the ribbon arrays are comparable to the losses in standard rectangular waveguides. The shaded area in this and subsequent figures has been inserted for illustrative comparison with the standard rectangular waveguides. Note that, in contrast to standard rectangular waveguides, the losses increase with frequency within the operating band.

Fig. 6 shows the excess loss factors of the corresponding slot arrays obtained by (27) and (29), which show that the losses per unit length are somewhat higher for this structure.

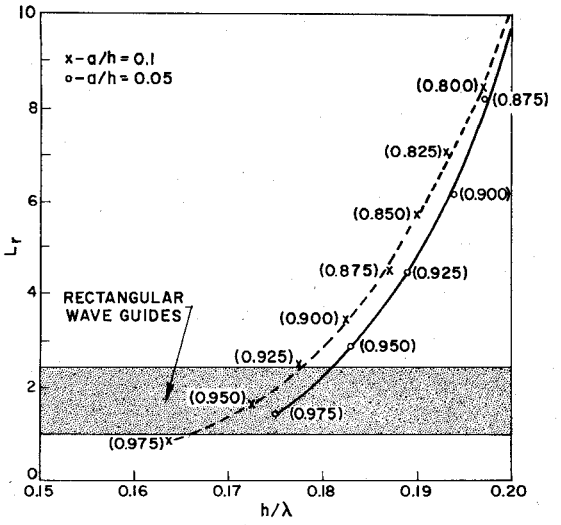

Fig. 7. Excess loss factor for metallic cylinders array. $d/\lambda = 0.2$. Corresponding values of v/c are in brackets.

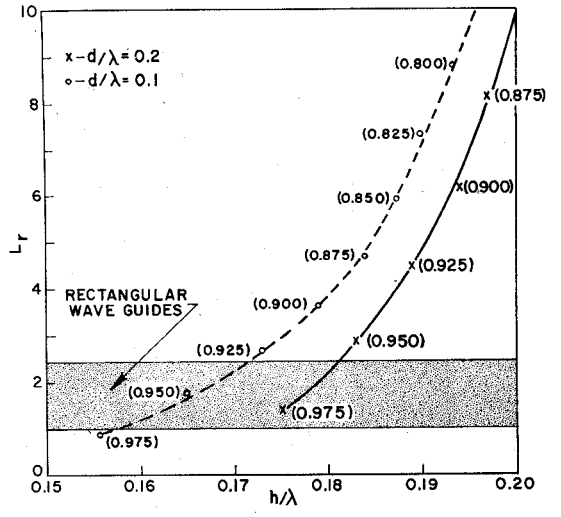

Fig. 8. Excess loss factor for metallic cylinders array. $a/h = 0.05$. Corresponding values of v/c are in brackets.

Figs. 7 and 8 show the dependence of L_r (or metallic-cylinders array) upon the parameters a/h and d/λ. For a given value of v/c, L_r increases with decreasing values of a/h, while L_r decreases with the decreasing values of d/λ (or D). The values of v/c were taken from Mailloux's [3] curves.

In the numerical computation of P_z in (25), we have observed that the zeroth-order ($m=0$) mode carried practically all the power of the bounded wave. Therefore, we can approximate M_1 by

$$M_1 \simeq \frac{|g_0|^2(v/c)^2}{D^2} \cdot \int_{-\infty}^{\infty} \frac{\left[\cos H \frac{\sin Hy}{Hy} - \cos Hy \frac{\sin H}{H}\right]^2}{(1-y^2)\left[1+\left(\frac{v}{c}\right)^2(y^2-1)\right]^{3/2}} dy. \quad (30)$$

From (24) with $\delta \to 1$ and low values of u_0, we obtain $M_3 \sim 2\pi/u_0 = d/a$. Utilizing these results in (26), we obtain

$$\alpha_r \simeq \frac{D}{(v/c)^2 a/h} Z \quad (31)$$

with Z being a function of H and not a very sensitive function of the parameters a/h, D, and v/c. Although (31) is a very approximate formula, it nevertheless indicates the proper relation and range of the various array parameters. Such a formula can serve as a guideline in exploring the proper combination of parameters that will minimize the relative power losses.

V. Conclusion

In this work we have developed the necessary formalism for the evaluation of the relative power losses in ribbon and slot arrays. The losses in these structures obey the same frequency-scaling characteristics as rectangular waveguides operated in the dominant mode. The losses of the cylinder and ribbon arrays are found to be comparable to rectangular waveguides. With a proper choice of parameters, the losses in the slot arrays can be brought to within a factor of 2 of the losses in rectangular waveguides. Additional reductions of the loss are desirable and may possibly result from special shaping of the slots (or ribbons) and specific choice of array dimensions.

Clearly, there will also be attenuation due to power scattered by deviations from the ideal periodic geometry. However, whereas the latter can be reduced by greater care in manufacture, the ohmic losses represent a more intrinsic limitation.

Appendix

Power Carried by the Bounded Wave in Ribbon Arrays

The electromagnetic field is obtained from (3) and (7) as

$$H_x = \frac{1}{\sqrt{8\pi}} \sum_{m=-\infty}^{\infty} \exp(j\beta_m z) \int_{-\infty}^{\infty} l_{mz} \exp(-a_m|y|) \exp(-jtx)dt \cdot \begin{cases} -1, & y>0 \\ 1, & y<0 \end{cases}$$

$$H_y = \frac{j}{\sqrt{8\pi}} \sum_{m=-\infty}^{\infty} \exp(j\beta_m z) \int_{-\infty}^{\infty} [\beta_m l_{mx} + t l_{mz}] \frac{\exp(-a_m|y|)}{a_m} \exp(-jtx)dt$$

$$H_z = -\frac{1}{\sqrt{8\pi}} \sum_{m=-\infty}^{\infty} \exp(j\beta_m z) \int_{-\infty}^{\infty} l_{mx} \exp(-a_m|y|) \exp(-jtx)dt \cdot \begin{cases} -1, & y>0 \\ 1, & y<0 \end{cases} \quad (32)$$

$$E_x = \frac{j\omega\mu}{\sqrt{8\pi}} \sum_{m=-\infty}^{\infty} \exp(j\beta_m z) \int_{-\infty}^{\infty} [l_{mx}(1 - t^2/k^2) + \beta_m l_{mz} t/k^2] \frac{\exp(-a_m | y |)}{a_m} \exp(-jtx)dt$$

$$E_y = \frac{\omega\mu}{\sqrt{8\pi}\, k^2} \sum_{m=-\infty}^{\infty} \exp(j\beta_m z) \int_{-\infty}^{\infty} [tl_{mx} - \beta_m l_{mz}] \exp(-a_m | y |) \exp(-jtx)dt \cdot \begin{cases} -1, & y > 0 \\ 1, & y < 0 \end{cases}$$

$$E_z = \frac{j\omega\mu}{\sqrt{8\pi}} \sum_{m=-\infty}^{\infty} \exp(j\beta_m z) \int_{-\infty}^{\infty} [(1 - \beta_m^2/k^2) l_{mz} + \beta_m l_{mx} t/k^2] \frac{\exp(-a_m | y |)}{a_m} \exp(-jtx)dt \tag{33}$$

where $a_m = \sqrt{\alpha_m^2 + t^2}$ and l_{mx} and l_{mz} are functions of the transform variable t.

The power carried by the bounded wave at plane z is

$$P_z = \frac{1}{2} \operatorname{Re} \left\{ \int\int_{-\infty}^{\infty} \boldsymbol{E} \times \boldsymbol{H}^* \cdot \hat{z} dx dy \right\} = \frac{1}{2} \operatorname{Re} \left\{ \int\int_{-\infty}^{\infty} [E_x H_y^* - E_y H_x^*] dx dy \right\}. \tag{34}$$

Upon the substitution of (32) and (33) in (34), and integrating with respect to x and y, we obtain

$$P_z = \frac{\omega\mu}{4} \operatorname{Re} \int_{-\infty}^{\infty} \sum_{n,m=-\infty}^{\infty} \sum \frac{\exp[j(\beta_m - \beta_n)z]}{a_m + a_n} \cdot \left\{ \frac{\beta_n(k^2 - t^2)}{k^2 a_m a_n} l_{mx} l_{nx}^* + \frac{\beta_m}{k^2} \left(1 + \frac{t^2}{a_m a_n}\right) l_{mz} l_{nz}^* + \frac{t}{k^2} \left[\frac{k^2 - t^2}{a_m a_n} - 1 \right] l_{mx} l_{nz}^* + \frac{t}{k^2} \frac{\beta_m \beta_n}{a_m a_n} l_{mz} l_{nx}^* \right\} dt. \tag{35}$$

With

$$\frac{1}{a_m + a_n} = \frac{j(a_m - a_n)}{(\beta_m + \beta_n) j(\beta_m - \beta_n)}$$

and

$$\frac{\exp[j(\beta_m - \beta_n)z]}{j(\beta_m - \beta_n)} = \frac{1}{j(\beta_m - \beta_n)} + \int_0^z \exp[j(\beta_m - \beta_n)z'] dz'$$

we obtain from (35)

$$P_z = P_z|_{z=0} + \operatorname{Re} \left[\frac{j\omega\mu}{4} \int_{-\infty}^{\infty} dt \int_0^z dz' \sum_{m,n=-\infty}^{\infty} \sum \exp[j(\beta_m - \beta_n)z'] \frac{(a_m - a_n)}{(\beta_m + \beta_n) k^2} \cdot \left\{ \frac{\beta_n(k^2 - t^2)}{a_m a_n} l_{mx} l_{nx}^* + \beta_m \left(1 + \frac{t^2}{a_m a_n}\right) l_{mz} l_{nz}^* + t \left(\frac{k^2 - t^2}{a_m a_n} - 1 \right) l_{mx} l_{nz}^* + t \frac{\beta_m \beta_n}{a_m a_n} l_{mz} l_{nx}^* \right\} \right]. \tag{36}$$

With

$$\frac{\beta_n}{\beta_m + \beta_n} \frac{a_m - a_n}{a_m a_n} = \frac{\beta_n}{a_n(\beta_m + \beta_n)} + \frac{\beta_m}{a_m(\beta_m + \beta_n)} - \frac{1}{a_m}$$

$$\frac{\beta_n}{\beta_m + \beta_n} (a_m - a_n) = a_m - \frac{\beta_m a_m}{\beta_m + \beta_n} - \frac{\beta_n a_n}{\beta_m + \beta_n}$$

and

$$\left(\frac{k^2 - t^2}{a_m a_n} - 1 \right) \frac{a_m - a_n}{\beta_m + \beta_n} = \frac{(\beta_n^2 - a_n^2)}{a_n(\beta_m + \beta_n)} - \frac{\beta_m^2 - a_m^2}{a_m(\beta_m + \beta_n)} - \frac{a_m - a_n}{\beta_m + \beta_n} = \frac{\beta_n^2}{a_n(\beta_m + \beta_n)} + \frac{\beta_m \beta_n}{a_m(\beta_m + \beta_n)} - \frac{\beta_m}{a_m}$$

we obtain from (36) after discarding the imaginary terms

$$P_z = P_z|_{z=0} + \operatorname{Re} \left[\frac{-j\omega\mu}{4} \int_{-\infty}^{\infty} dt \int_0^z dz' \sum_{m,n=-\infty}^{\infty} \sum \frac{\exp[j(\beta_m - \beta_n)z']}{k^2 a_m} \cdot \{ (k^2 - t^2) l_{mx} l_{nx}^* + (t^2 - a_m^2) l_{mz} l_{nz}^* + \beta_m t (l_{mx} l_{nz}^* + l_{mz} l_{nx}^*) \} \right]. \tag{37}$$

Using (32) and (33), (37) is reduced to

$$P_z = P_z\Big|_{z=0} + 2 \left\{ \frac{1}{2} \operatorname{Re} \int_{x=-h}^{h} \int_0^z \boldsymbol{E} \times \boldsymbol{H}^* \cdot \hat{y} dx dz' \Big|_{y=0} \right\}. \tag{38}$$

Since $\boldsymbol{E}_t$ vanishes on the metallic strip, P_z is independent of z. By setting $m = n$ in (35), we obtain P_z as

$$P_z = \text{constant} = \frac{\omega\mu}{8} \operatorname{Re} \int_{-\infty}^{\infty} dt \sum_{m=-\infty}^{\infty} \frac{1}{k^2 a_m^3} \cdot \{ \beta_m [(k^2 - t^2) | l_{mx} |^2 + (a_m^2 + t^2) | l_{mz} |^2] + t(k^2 - t^2 - a_m^2) l_{mx} l_{mz}^* + t\beta_m^2 l_{mz} l_{mx}^* \}. \tag{39}$$

ACKNOWLEDGMENT

The authors wish to thank Dr. E. R. Nagelberg for his critical reading of the manuscript and for many stimulating discussions, Miss A. M. Russell and Miss D. M. Czahla for their assistance in the numerical computation, and Miss A. P. Irwin for her assistance in the graphical presentation.

REFERENCES

[1] D. L. Sengupta, "On the phase velocity of wave propagation along an infinite Yagi structure," *IRE Trans. Antennas Propagat.*, vol. AP-7, pp. 234–239, July 1959.
[2] J. Shefer, "Periodic cylinder arrays as transmission lines," *IEEE Trans. Microwave Theory Tech.*, vol. MTT-11, pp. 55–61, Jan. 1963.
[3] R. J. Mailloux, "Antenna and wave theories of infinite Yagi–Uda arrays," *IEEE Trans. Antennas Propagat.*, vol. AP-13, pp. 499–506, July 1965.
[4] E. R. Nagelberg and J. Shefer, "Dispersion characteristics of an array of parasitic linear elements," *IEEE Trans. Microwave Theory Tech.*, vol. MTT-14, pp. 391–396, Aug. 1966.
[5] V. N. Ivanov, "Surface waves in a semi-infinite array," *Radio Eng. Electron. Phys.*, vol. 14, no. 3, pp. 350–354, 1969.
[6] ——, "Surface waves in a semi-infinite ribbon array," *Radio Eng. Electron. Phys.*, vol. 14, no. 10, pp. 1520–1525, 1969.
[7] P. N. Butcher, "The coupling impedance of tape structures," *Proc. Inst. Elec. Eng.*, ser. B, vol. 104, pp. 177–187, Mar. 1957.
[8] L. C. Shen, "Possible new applications of periodic linear arrays," *IEEE Trans. Antennas Propagat.* (Commun.), vol. AP-18, pp. 698–699, Sept. 1970.
[9] R. E. Collin, *Field Theory of Guided Waves*. New York: McGraw-Hill, 1960, chs. I and IX.
[10] N. Marcuvitz, *Waveguide Handbook* (Radiation Laboratory Series), vol. 10. New York: McGraw-Hill, 1951, chs. I and II.
[11] P. M. Morse and H. Feshbach, *Methods of Theoretical Physics*. New York: McGraw-Hill, 1953, ch. IV.
[12] I. M. Ryzhik and I. S. Gradshteyn, *Tables of Integrals, Series and Products*. New York: Academic Press, 1965, p. 387.

Microwave Integrated Oscillators for Broad-Band High-Performance Receivers

HERMAN C. OKEAN, SENIOR MEMBER, IEEE, EUGENE W. SARD, SENIOR MEMBER, IEEE, AND ROBERT H. PFLIEGER, MEMBER, IEEE

***Abstract*—The design and development of a variety of microwave integrated circuit oscillators for use in integrated broad-band high-performance receiving systems is described. Examples of various thin-film microstrip oscillators directed to this application are provided including: 1) fixed-frequency Gunn-effect oscillators covering C to K_u band; 2) X-band varactor-tuned Gunn-effect oscillators providing up to 15 percent tuning bandwidth; 3) S-band step-tuned transistor oscillator assembly with better than half-octave digital tuning range; 4) L-band varactor-tuned transistor oscillator with almost an octave tuning range.**

I. INTRODUCTION

THIS PAPER describes the design and development of a variety of microwave integrated circuit (MIC) oscillators for use in integrated broad-band high-performance receivers. The role of these oscillators in such receivers, the impact of MIC technology on their construction, and specific embodiments of MIC oscillators operating from L to K_u band are included.

Manuscript received February 24, 1971; revised June 1, 1971. This work was supported by the Air Force Avionics Laboratory (Advanced Electronic Devices Branch), Wright-Patterson Air Force Base, Dayton, Ohio, under Contract F-33615-69-C-1859.

H. C. Okean was with AIL, Division of Cutler-Hammer, Melville, N. Y. He is now with LNR Communications, Inc., Farmingdale, N. Y. 11735.
E. W. Sard and R. H. Pflieger are with AIL, Division of Cutler-Hammer, Melville, N. Y. 11746.

II. GENERAL ASPECTS OF MIC OSCILLATOR DESIGN

The application of MIC oscillators to broad-band high-performance receivers is primarily as electronically tunable local oscillators for repetitively swept [1], step-scanned [2], [3], or adaptively tunable superheterodyne receiver channels. Of the various oscillator types relevant to this application [1]–[8] in the L- to K_u-band frequency range, those which will be described here include:

1) Fixed-frequency C- to K_u-band Gunn-effect oscillators, which are designed for incorporation in a corporate-switched combining array. This configuration, therefore, constitutes a digitally addressed step-tunable C- to K_u-band LO assembly for step-scanned superheterodyne receiver application.

2) Digitally addressed S-band step-tuned transistor oscillator-driven LO assembly for step-scanned superheterodyne receiver application. A switched reactive array constitutes the digitally tunable resonator for the step-tuned transistor oscillator.

3) Varactor-tuned X-band GEOs which serve as continuously tunable LOs for adaptively tunable superheterodyne receiver applications.

4) Varactor-tuned L-band transistor oscillator for